Article

Research on a Hierarchical Control Strategy for Anti-Lock Braking Systems Based on Active Disturbance Rejection Control (ADRC)

Shi Luo, Bing Zhang *, Jiantao Ma and Xinyue Zheng

School of Automotive and Traffic Engineering, Jiangsu University, Zhenjiang 212013, China;
luoshi@ujs.edu.cn (S.L.); 17696853582@163.com (J.M.); 2212404006@stmail.ujs.edu.cn (X.Z.)
* Correspondence: 2222304033@stmail.ujs.edu.cn; Tel.: +86-159-5135-8539

Abstract: To improve the slip rate control effect for different road conditions during emergency braking of wheel hub motor vehicles, as well as to address the problems of uncertainty and nonlinearity of the system when the electro-mechanical braking system is used as the actuator of the ABS, a hierarchical control strategy of the anti-lock braking system (ABS) using active disturbance rejection control (ADRC) is proposed. Firstly, a vehicle dynamics model and an ABS model based on the EMB system are established; secondly, a speed observer based on the dilated state observer is used in the upper layer to design a pavement recognition algorithm, which recognizes the current pavement and outputs the optimal slip rate; then, an ABS controller based on the ADRC algorithm is designed for the lower layer to track the optimal slip rate. In order to verify the performance of the pavement recognition method and control strategy, vehicle simulation software is used to establish the model and simulation. The results show that the road surface recognition method can quickly and effectively recognize the road surface, and comparing the emergency braking control effects of PID and SMC under different road surface conditions, the ADRC strategy has better robustness and reliability, and improves the braking effect.

Keywords: active disturbance rejection control; slip rate control; road recognition; electro-mechanical brake; distributed vehicle control

1. Introduction

With the development of automobile electrification and intelligence, the brake-by-wire (BBW) system has received more and more attention. This system can be divided into two kinds: electro-hydraulic brake (EHB) and electro-mechanical brake (EMB).The EHB system adopts electronic control to replace part of the mechanical control, retaining part of the hydraulic components, and exists as a transitional technology with slow braking response and complex piping arrangement [1–3]. The EMB system provides a more advanced braking program compared with the former; the EMB system does not require a hydraulic system, and is driven directly by the motor to generate braking force, with a faster braking response, a small system size, a simple structure, ease of installing and maintenance, ease of integration of the parking brake, and so on. The flexibility and modular design of distributed drive systems provide ideal conditions for the integration of electro-mechanical brakes (EMBs), and their combination offers significant advantages [4–6].

The anti-lock braking system (ABS) uses the slip rate of the wheels as the controlled object, keeps the slip rate near the optimal slip rate, avoids the tire locking phenomenon when the wheels have a large braking torque, and improves the braking performance of the vehicle [7–9]. The use of the EMB system in combination with the traditional ABS can more

accurately control the braking force of the wheels, maintain the optimal slip rate of the wheels, improve the performance of the ABS, and ensure that the vehicle always maintains the ability to steer, which is an important safeguard for the safety of driving the vehicle [10]. However, vehicle braking effectiveness is affected by the tire–road friction coefficient and controller robustness, which provide challenges to improving braking effectiveness. Numerous scholars have conducted extensive research on the above problems. In terms of pavement identification, Wang [11] used a combination of strong tracking traceless Kalman filtering and interactive multi-model traceless Kalman filtering to estimate the road friction coefficient, which has good identification accuracy. In the literature [12], an identification method using machine learning and a bi-radial basis function neural network to build a pavement adhesion coefficient estimator using the Extended Kalman Filter is proposed, but there are significant fluctuations in the simulated pavement adhesion coefficients. Sun proposed a fusion algorithm based on improved singular-value decomposition trace-free Kalman filtering for estimating the tire–road friction coefficient [13].

At the same time, ABS controller robustness and tire slip rate control are also important factors in braking effectiveness; the current automotive ABS mainly involves PID control and integral sliding-mode control (SMC) [14]. An optimized fuzzy adaptive PID algorithm is proposed in the literature [15] to improve the braking stability of the ABS. Salma [16] proposed a global sliding-mode controller and utilized the Lyapunov method to establish system stability, aiming to minimize the error between the actual slip rate and the optimal slip rate. However, both of these have problems, such as poor adaptability and jitter. In the literature [17], an H∞ gain-scheduling controller is proposed, which can maintain the slip ratio within the optimal range according to road conditions, thereby achieving optimal braking performance. Auto-Disturbance Control (ADRC), with the advantages of fast response, strong decoupling, model-independence, high control accuracy, estimation of internal and external disturbances, and compensation [18], is widely used in motor control [19], trajectory tracking [20] and other fields. In the literature [21], ADRC is applied to a line-controlled braking system to analyze its effect on ABS control, but the effects of the optimal slip rate and EMB on braking performance are not studied in depth.

Based on the above existing problems, considering the effects of the variability of different road surface attachments and controller robustness on the ABS braking effect, this paper proposes a hierarchical control strategy for the ABS using self-impedance control. Firstly, a road surface identification method based on real-time estimation of longitudinal speed by an extended state observer (ESO) is proposed to output the optimal slip rate, and this is used as the control objective to design the ABS control system, based on the ADRC strategy. Finally, the effectiveness of the control strategy, as well as of the pavement identification method, is verified through simulation experiments in different road environments.

The structure of this paper is as follows. In Section 2, the vehicle dynamics model and tire pavement model are introduced. In Section 3, the longitudinal speed observer and the road surface identification method are established to obtain the optimal slip rate. In Section 4, an ADRC-based ABS control strategy is designed to control the wheel slip rate so that it is stabilized at the optimal slip rate. Section 5 carries out the simulation verification of the road surface recognition method and ABS control system, and analyzes and compares the braking effect of the three control methods on single and variable road surfaces. Finally, conclusions are given in Section 6.

2. Vehicle Model

2.1. Vehicle Dynamics Model

To simplify the analysis, the effects of rolling resistance and grade resistance are neglected, and a single-wheel model is used as the basis for studying the problem. Figure 1 shows a schematic diagram of the braking forces; its dynamics equations are as follows [22]:

$$m\dot{v} = -F_{xb} \tag{1}$$

$$J\dot{\omega} = F_{xb}R - T_b \tag{2}$$

$$F_{xb} = \mu(\lambda)F_z \tag{3}$$

The slip rate is defined as follows:

$$\lambda = \frac{v - \omega R}{v} \tag{4}$$

where m is one-quarter of the total mass of the vehicle, v is the longitudinal speed, F_{xb} is the ground braking force, J is the wheel moment of inertia, R is the tire radius, T_b is the brake torque, and ω is the angular velocity of the wheels, and here, $\dot{\omega}$ for the angular deceleration of the wheels.
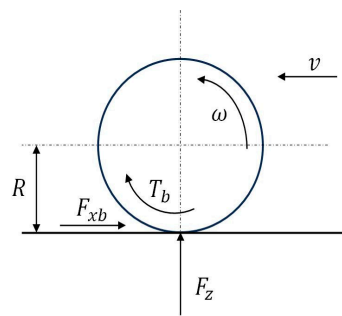

Figure 1. Braking force diagram.

2.2. Tire–Pavement Model

The mathematical tire model established by Burckhardt [23] can accurately represent the longitudinal adhesion relationship between the tire and the road surface during vehicle braking. The expression for this model is as follows:

$$\mu(\lambda) = c_1[1 - exp(-c_2\lambda)] - c_3\lambda \tag{5}$$

where c_1, c_2, c_3 are the fitting parameters for each typical road surface, as well as the optimal slip rate and adhesion coefficient for six different road surfaces [24], as shown in Table 1.

Table 1. Fitted parameter values for typical road surfaces.

	c_1	c_2	c_3	λ_{ref}	μ_{max}
Dry asphalt	1.2801	23.99	0.52	0.17	1.17
Dry cement	1.1973	25.168	0.5373	0.16	1.09
Wet asphalt	0.857	33.822	0.347	0.13	0.8013
Cobblestone	0.4004	33.708	0.1204	0.14	0.34
Snow	0.1946	94.129	0.0646	0.06	0.1907
Ice	0.05	306.39	0.001	0.03	0.05

3. Design of Road Surface Identification Methods

During the braking process, the influence of brake system factors is assumed to be consistent; therefore, the tire–road friction coefficient conditions become the primary factor affecting braking performance. Additionally, the tire–road friction coefficient provides a crucial basis for the design of road surface recognition methods, due to its variability.

3.1. Velocity Observer

The basic idea of the dilated state observer is as follows: the total perturbation is dilated into a new state variable of the system, and the inputs and outputs of the system are utilized to observe the state variable of the system and the perturbation to which it is subjected [25].

Combining Equations (1) and (2), the following can be obtained:

$$\dot{\omega} = -\frac{mR\dot{v}}{J} - \frac{T_b}{J} \tag{6}$$

In practical situations, there exist model errors and external disturbances, denoted as $\rho(t)$. Therefore, we can obtain the following:

$$\dot{\omega} = -\frac{mR\dot{v}}{J} + \rho(t) - \frac{T_b}{J} \tag{7}$$

Since precise speed information cannot be obtained [26,27], the term containing speed information, $-\frac{mR\dot{v}}{J} + \rho(t)$, is considered as an external unknown total disturbance to the system, and is expanded into a new state variable, x_2. The state equation takes the following form:

$$\begin{cases} \dot{x}_1 = x_2 + bu \\ \dot{x}_2 = h \\ y = x_1 \end{cases} \tag{8}$$

where $x_1 = \omega$, $x_2 = -\frac{mR\dot{v}}{J} + \rho(t)$ is the aggregate disturbance, and h is derivative of the disturbance; $b = -\frac{1}{J}$, $u = T_b$, the angular velocity ω and the braking torque T_b are used as inputs to the system.

The extended state observer is designed according to Equation (8), as follows:

$$\begin{cases} \dot{z}_1 = z_2 - \beta_1 f_{al}(\varepsilon, 0.5, \delta) + bu \\ \dot{z}_2 = -\beta_2 f_{al}(\varepsilon, 0.25, \delta) \\ \varepsilon = z_1 - y \end{cases} \tag{9}$$

where z_1 and z_2 are observed values of x_1 and x_2, respectively. ε is the difference between the observed value z_1 and the input value y. β_1 and β_2 are parameters of the controller; after testing, it was determined that $\beta_1 = 80$ and $\beta_2 = 14000$. The interval length δ is set to 0.1. The function f_{al} is represented as follows [28]:

$$f_{al}(\varepsilon, \alpha, \delta) = \begin{cases} \varepsilon \delta^{\alpha-1} & , \quad |\varepsilon| \leq \delta \\ sign(\varepsilon)\big|\varepsilon\big|_\alpha & , |\varepsilon| > \delta \end{cases} \tag{10}$$

The above state observer obtains an observation z_2 for x_2, where z_2 contains the integral of the longitudinal vehicle velocity $\dot{v}$. The expression is obtained as follows:

$$z_2 = -\frac{mR\dot{v}}{J} + \rho(t) \tag{11}$$

At the start of braking, the longitudinal vehicle speed and wheel speed are approximately equal. The initial speed of the vehicle is assumed as v_0. The longitudinal speed observation is given by the following:

$$\hat{v} = \int \left(\hat{\dot{v}} + v_0 \right) dt = \int [-\frac{z_2 J}{mR} + \rho(t) + v_0] dt \tag{12}$$

3.2. Road Surface Identification

The tire, as the medium of contact between the vehicle and the road, transmits the forces and torques required for vehicle motion. During braking, the tangential force experienced by the vehicle is limited, due to varying degrees of slip between the tire and the ground. The maximum longitudinal braking force F_{xbmax} is given by the following:

$$F_{xbmax} = \mu_{max} F_z \tag{13}$$

Based on Equations (2) and (3), the longitudinal adhesion utilization coefficient of the wheel can be obtained as follows:

$$\mu = \frac{J\dot{\omega} + T_b}{F_z R} \tag{14}$$

The braking torque in the equation is obtained from the EMB (electro-mechanical brake) actuator model, while the wheel angular deceleration $\dot{\omega}$ is acquired through wheel speed sensors.

The vehicle speed $\hat{v}$ is obtained from the longitudinal vehicle speed observer. Using Equation (4), the slip ratio λ is calculated. Based on the Burckhardt tire model, the theoretical adhesion coefficients μ_i ($\square = 1,2,3,4,5,6$) for six typical road conditions are derived for this slip ratio. These theoretical values are then compared with the actual adhesion coefficient μ_r. The following function is designed to perform this comparison:

$$Min = Min|\mu_r - \mu_i| \tag{15}$$

The *Min* function is calculated in real time during braking, and when the closest road surface is finally found, the initial recognition is completed, and the optimal slip rate of the current road surface is output, as shown in Figure 2.
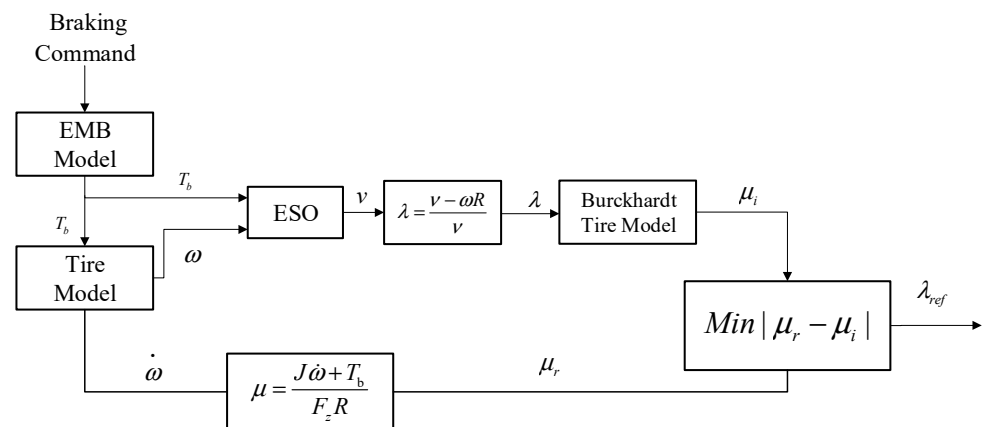

Figure 2. Flowchart of road surface identification method.

4. ADRC-Based ABS Slip Ratio Tracking Control

The ABS is often used in extreme conditions of vehicle driving, and is susceptible to external disturbances, so the ABS control algorithm is required to have the advantages of fast response and strong resistance to external disturbances. Self-immunity control has the

unique advantages of not relying on the precise model of the controlled object, as well as the estimation and compensation for internal and external disturbances, which can effectively inhibit the external interference and fast response, and are suitable for nonlinear control systems, which can effectively improve control quality and control accuracy. Therefore the self-immunity control theory is chosen for the design of the ABS controller.

4.1. ABS Model

4.1.1. EMB Selection

In this paper, the floating caliper disk structure type model from Ref. [29] is used, including the following components, as shown in Figure 3: a drive motor, a planetary gear mechanism, a ball screw mechanism, and a brake disk. The braking torque equations are shown in (2) to (3).

$$T_b = \begin{cases} 0, & \left|T_e\right| < T_f \\ K_b(K_t I_a - T_f), & \left|T_e\right| \geq T_f \end{cases} \tag{16}$$

$$K_b = \frac{4\pi i_x \eta_x \eta_s \mu_b r_b}{P_h} \tag{17}$$

where T_e is the electromagnetic torque of the drive motor, T_f is the friction torque of the drive motor, K_t is the motor torque coefficient of the wheel brake, K_b is the output torque coefficient of the brake, I_a is the armature current of the motor, i_x is the planetary gear ratio, η_s is the mechanical efficiency of the ball screw, μ_b is the coefficient of friction of the brake disk, r_b is the effective radius of the brake disk, P_h is the lead of the ball screw, and η_x is the mechanical efficiency of the planetary gears.
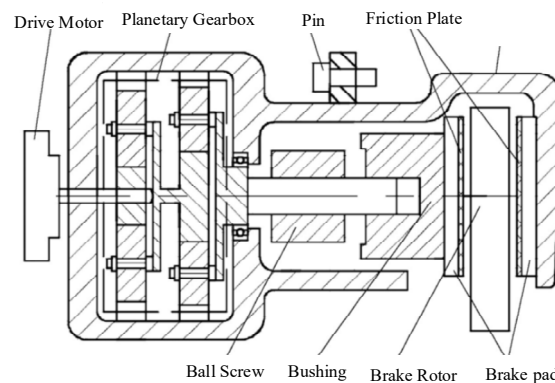

Figure 3. Electromechanical brake actuator structure.

4.1.2. Slip Rate Dynamic Model

To find the second derivative of the wheel slip ratio described by Equation (4), the following expression is derived:

$$\ddot{\lambda} = -\frac{\ddot{\omega}R}{v} + \frac{\omega\ddot{v}R}{v^2} + \frac{2\dot{\omega}\dot{v}R}{v^2} - \frac{2\omega\dot{v}^2 R}{v^3} \tag{18}$$

By combining Equations (1)–(4) and Equations (6) and (7), and substituting them into the above equation, we can obtain the second-order nonlinear system expression for the slip ratio:

$$\ddot{\lambda} = \frac{1}{mv}\left((\lambda - 1)F\dot{\mu}(\lambda) + 2F_z\mu(\lambda)\dot{\lambda} - \tau F_z R^2\dot{\mu}(\lambda) + \tau K_b K_t R\dot{I}_a\right) \tag{19}$$

where $\tau = m/J$; the dynamic model of the ABS slip rate of the EMB system can be described as a second-order nonlinear system with respect to slip rate.

To improve vehicle braking performance, an active disturbance rejection control (ADRC) algorithm was used to design a controller for tracking the optimal slip ratio. Figure 4 shows the structure diagram of the ADRC-based ABS control strategy.
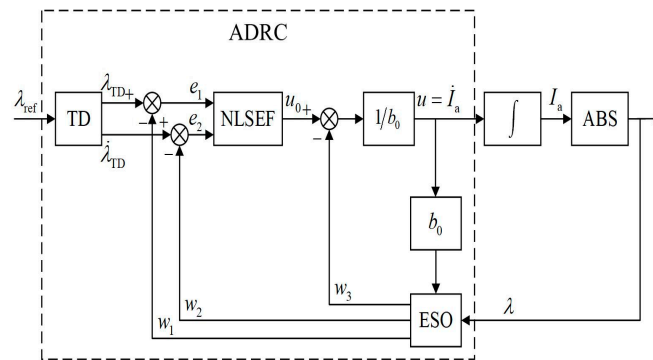

Figure 4. Structure of ABS control strategy in ADRC.

4.2. Design of ADRC

The active disturbance rejection control (ADRC) system comprises three main components: the tracking differentiator (TD), the extended state observer (ESO), and the nonlinear state error feedback (NLESF) [30].

4.2.1. Extended State Observer (ESO) Design

The ESO is utilized to estimate both the state variables and the overall disturbance within the system. Equation (19) is recast into a state equation representation, as follows:

$$\begin{cases} \dot{\theta}_1 = \theta_2 \\ \dot{\theta}_2 = \theta_3 + bu \\ \dot{\theta}_3 = h \\ y_1 = \theta_1 = \lambda \end{cases} \tag{20}$$

where λ is the true slip rate, $\theta_3 = f = \frac{1}{mv}[(\lambda - 1)F_z\mu_{(\lambda)} + 2F_z\mu_{(\lambda)}\dot{\lambda} - \tau F_z R^2 \dot{\mu}(\lambda)]$ is the new expansion state variable, is the total perturbation, h is the differential value of the total perturbation, $b = \tau K_b K_t R$, and $\dot{I}_a$ is the differential value of the current.

From (14), the extended state observer formula can be obtained, as follows:

$$\begin{cases} \varepsilon = z_1 - y \\ \dot{z}_1 = z_2 - \gamma_1 \varepsilon \\ \dot{z}_2 = z_3 - \gamma_2 f_{al}(\varepsilon_1, 0.5, \delta_1) + bu \\ \dot{z}_3 = -\gamma_3 f_{al}(\varepsilon_1, 0.25, \delta_1) \end{cases} \tag{21}$$

where z_1, z_2, and z_3 are the observations of θ_1, θ_2 and θ_3, respectively; γ_1, γ_2, and γ_3 are the parameters of the controller; and the function f_{al} is as above.

4.2.2. Tracking Differentiator (TD) Design

The optimal slip ratio obtained from the upper-level road surface recognition method serves as the target slip ratio for the transitional process. The tracking differentiator (TD) is capable of smoothing input signals, filtering out high-frequency noise, while rapidly tracking the trend of signal changes and estimating the differential value of the signal. This results in obtaining the tracking signal and differential signal of the target slip ratio,

simultaneously serving to alleviate overshoot and oscillations. The tracking equation for the target slip ratio B is as follows:

$$
\begin{cases}
f_h = f_{han}[\lambda_{\mathrm{TD}}(k) - \lambda_{\mathrm{ref}}(k), \dot{\lambda}_{\mathrm{TD}}(k), r_0, h_0] \\
\lambda_{\mathrm{TD}}(k+1) = \lambda_{\mathrm{TD}}(k) + h\dot{\lambda}_{\mathrm{TD}}(k) \\
\dot{\lambda}_{\mathrm{TD}}(k+1) = \dot{\lambda}_{\mathrm{TD}}(k) + hf_h
\end{cases}
\tag{22}
$$

where λ_{ref} is the target slip rate output by the upper pavement recognition module; λ_{TD} and $\dot{\lambda}_{TD}$ are the tracking signal and its differential signal of λ_{ref}, respectively; r_0 is the velocity factor; and h_0 is the sampling step. According to [31], the f_h function can be expressed as follows:

$$
f_h = f_{han}(c_1, c_2, r_0, h_0)
\tag{23}
$$

$$
\begin{cases}
d = r_0 h_0{}^2 \\
a_0 = h_0 c_2 \\
y = c_1 + a_0 \\
a_1 = \sqrt{d(d + 8|y|)} \\
a_2 = a_0 + sign(y)(a_1 - d)/2 \\
s_y = [sign(y+d) - sign(y-d)]/2 \\
a = (a_0 + y - a_2)s_y + a_2 \\
s_a = [sign(a+d) - sign(a-d)]/2 \\
f_{han} = -r_0[a/d - sign(a)]s_a - r_0 sign(a)
\end{cases}
\tag{24}
$$

4.2.3. Nonlinear State Error Feedback (NLESF) Design

NLSEF uses a nonlinear combination designed to compensate for the total perturbations estimated in real time in ESO [32], ensuring that the system states stably converge to the desired equilibrium point. The nonlinear combination takes the following form:

$$
\begin{cases}
e_1 = \lambda_{\mathrm{TD}} - z_1 \\
e_2 = \lambda_{\mathrm{TD}} - z_2 \\
u_0 = \beta_1 f_{al}(e_1, \alpha_1, \delta_2) + \beta_2 f_{al}(e_2, \alpha_2, \delta_2)
\end{cases}
\tag{25}
$$

where β_1 and β_2 are controller parameters.

The calculation formula of the control volume formed by the system perturbation compensation can be obtained, as follows:

$$
u = \frac{u_0 - z_3}{b_0} = \dot{I}_a
\tag{26}
$$

where $-\frac{z_3}{b_0}$ is the component of the compensation disturbance, $\frac{u_0}{b_0}$ is the nonlinear feedback to control the integrator series-type component, and b_0 is the compensation factor, which is taken as b in the calibration process.

5. Simulation and Discussion

To verify the reliability and effectiveness of the proposed hierarchical ABS control strategy, an overall control strategy model was built in MATLAB/Simulink. The general design of the ABS control system is shown in Figure 5. Under emergency braking conditions, the road surface identification outputs the target slip ratio λ_{ref}. The ABS controller based on the ADRC algorithm is used to track the target slip ratio, and the output current controls the EMB actuator. The vehicle simulation conditions are set to emergency braking scenarios on different road surfaces with an initial braking speed of 20 m/s, and white noise is added to simulate real-world disturbances. The performance of the longitudinal vehicle

speed observer, the accuracy of the road surface identification method, and the braking effectiveness of the ABS control strategies using the PID, SMC (sliding-mode control), and ADRC methods are verified, respectively. Tables 2 and 3 provide the vehicle model parameters and controller parameters.
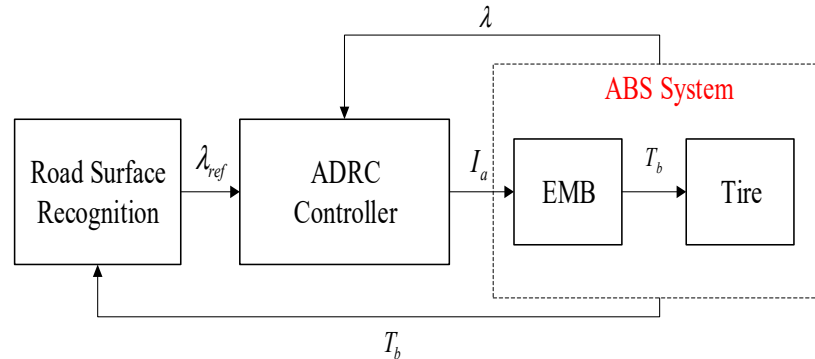

Figure 5. The framework of the ADRC-based ABS control system.

Table 2. Model parameters.

Parameters	Symbol	Value
Vehicle mass	m	$1800/4$ kg
Wheel rolling radius	R	0.3 m
Wheel rotational inertia	J	$0.9 \, \text{kg} \cdot \text{m}^2$
Vehicle wheelbase	L	2.8 m
Center of gravity height	h	0.45 m
Front braking constant	k_{bf}	300 Nm/MPa
Rear braking constant	k_{br}	200 Nm/MPa
Motor torque coefficient	K_T	$0.563 \, \text{N} \cdot \text{m} \cdot \text{A}^{-1}$
Motor friction torque	T_s	$0.1168 \, \text{N} \cdot \text{m}$
Planetary gear ratios	i_x	19
Efficiency of planetary gears	η_x	0.95
Ball Screw Efficiency	η_s	0.95
Ball Screw Guide	P_h	0.005
Effective radius of brake disk	r_b	0.12
Brake disk friction coefficient	μ_b	0.4

Table 3. Controller parameters.

Controller	Parameter	Value
PID	Proportional parameter Integral parameter Differential parameter	$K_p = 1.5$ $K_i = 50$ $K_d = 0.01$
SMC	Constant Velocity Approach Coefficient Exponential Convergence Coefficient	$\varepsilon = 20$ $q = 0.001$
ADRC	ESO	$\gamma_1 = 1000$ $\gamma_2 = 32{,}000$ $\gamma_3 = 680{,}000$ $\delta_1 = 0.01$
	TD	$r_0 = 100{,}000$ $h_0 = 180$
	NLESF	$\alpha_1 = 0.1$ $\alpha_2 = 1.75$ $\delta_2 = 0.01$

5.1. Pavement Recognition Simulation

In order to verify the effectiveness and accuracy of the road recognition method, two kinds of road surfaces, dry cement and snow, were selected for recognition verification, and the simulation condition was that the braking started at a wheel speed of 20 m/s.

Figure 6a shows the speed curve on a dry cement road; it can be seen that from the beginning of braking, the accuracy error of the observer slowly increases, and finally stabilizes at about 0.4 m/s. Figure 6b shows the speed curve on a snowy road; here, the observer's observation error slowly increases with the observation time, and finally stabilizes at 0.6 m/s. When the actual speed is lower than 2 m/s, the sensor receives weakened signal strength and the ambient noise becomes relatively more significant, resulting in a decrease in the signal-to-noise ratio, making it more difficult to extract accurate speed information from the signal; at the same time, the speed is too low, which makes the number of pulses generated by the wheel speed sensor per unit of time decrease, which can lead to insufficient resolution and affect the observations. In addition, the increase in error is due to the fact that the observer is always running during the braking process, resulting in there being some cumulative error. Figure 6c,d show the recognition results of dry concrete and snow pavement, respectively, where the pavement is recognized near 0.2 s and the optimal rate and maximum adhesion coefficient of the current pavement are outputted; meanwhile, at 0.2 s, the speed observation error is so small that it can be ignored.
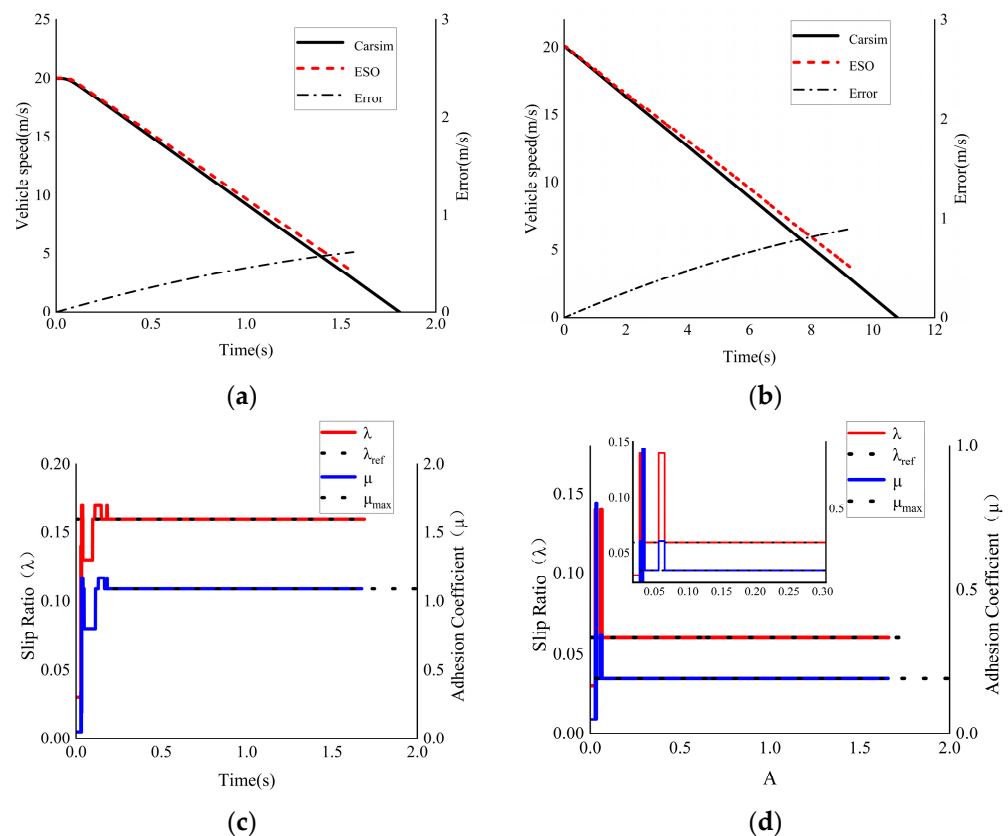

Figure 6. Simulation results of pavement identification. (**a**) Speed observation on dry cement road. (**b**) Speed observation on snowy road. (**c**) Dry cement road recognition. (**d**) Snow road recognition.

5.2. ABS Control System Simulation

5.2.1. Dry Cement Pavement Braking

Figure 7 shows the braking effect of the three ABS control strategies, ADRC, SMC, and PID, on dry concrete road. From Figure 7a, it can be seen that the braking distance

under the ADRC strategy is less than under the SMC and PID control strategies. Figure 7b,c shows that the ADRC strategy can produce a smooth and fast decrease in speed, which is better than the SMC and PID control. In terms of slip rate control, as shown in Figure 7d, neither ADRC nor SMC showed overshooting, and PID showed overshooting; the response time of ADRC to reach the steady state value was faster than that of SMC and PID, and there was no wheel holding phenomenon. The results show that the ABS under the control of the ADRC algorithm has better braking performance and improves the braking effect on dry cement road.
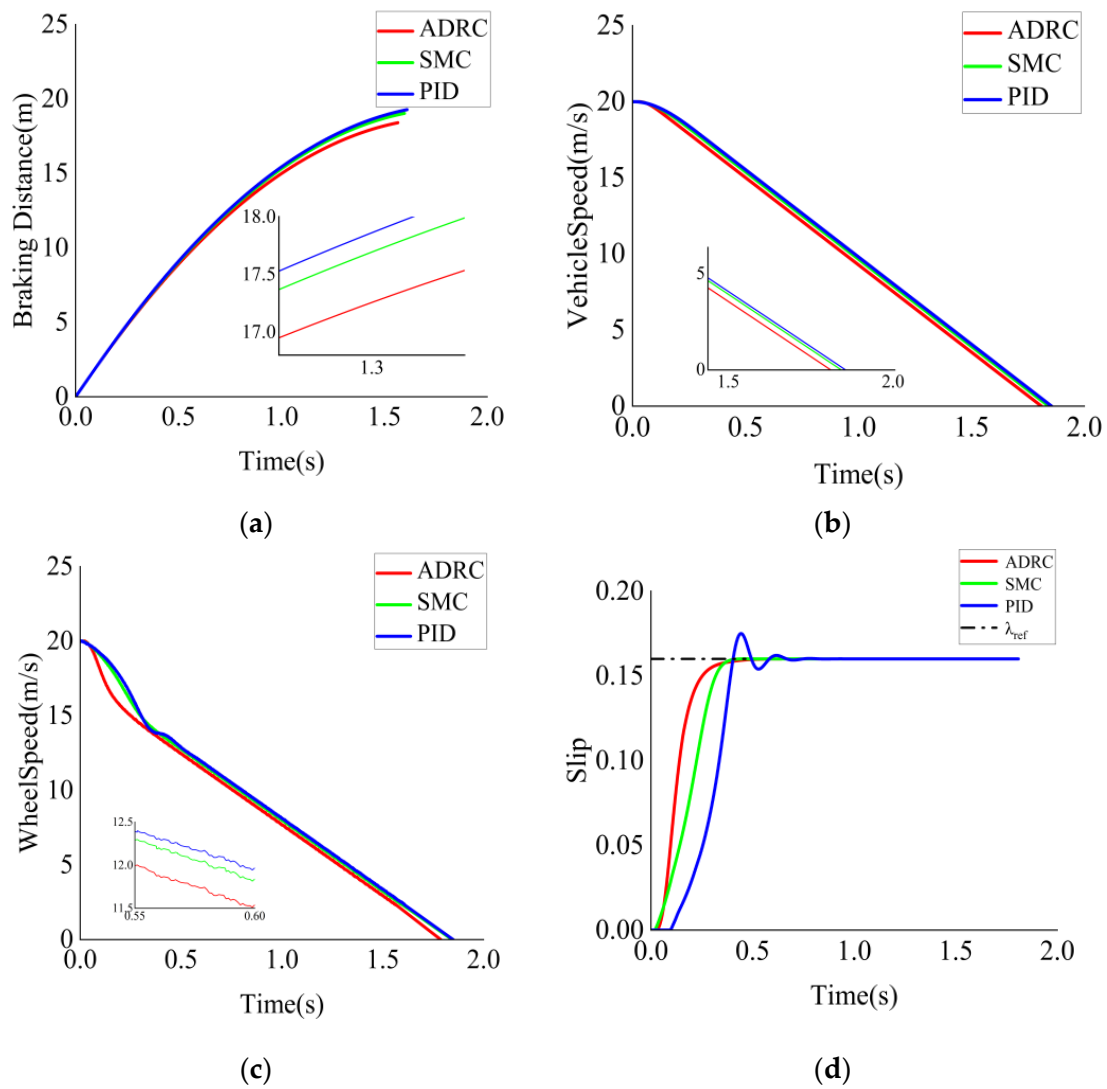
Figure 7. Braking performance on dry cement pavement. (**a**) Braking distance. (**b**) Vehicle speed. (**c**) Wheel speed. (**d**) Slip.

5.2.2. Snowy Pavement Braking

Figure 8 shows the braking effect of the three ABS control strategies, ADRC, SMC, and PID, on a snowy road surface. From Figure 8a, it can be seen that the braking distance under the ADRC strategy is the smallest, but the differences among the three strategies are minor, around 0.2 m. Figure 8b,c indicates that the difference in braking time between ADRC and SMC is negligible, with neither exceeding 11 s, while the braking time for PID is the longest, surpassing 11 s.
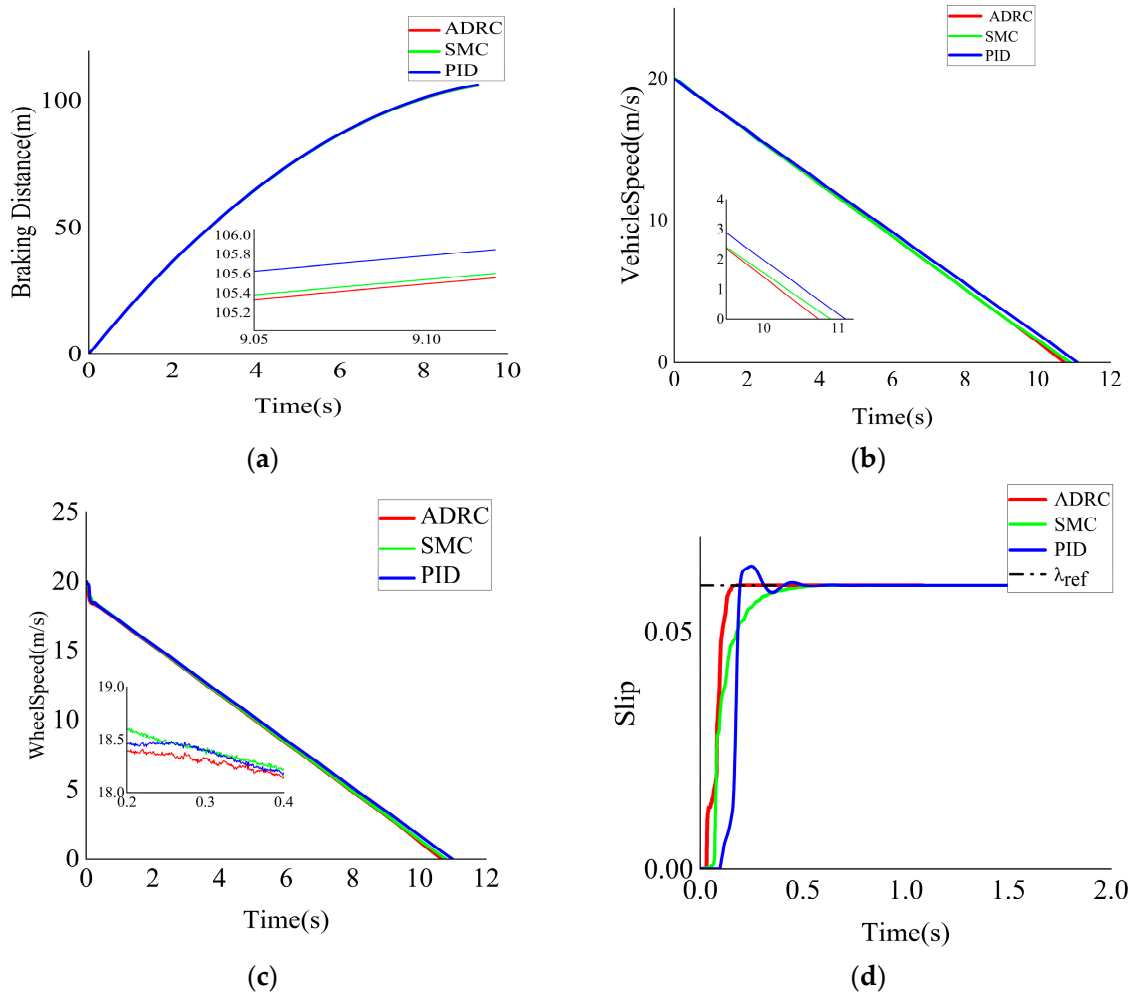
Figure 8. Braking performance on snowy pavement. (**a**) Braking distance. (**b**) Vehicle speed. (**c**) Wheel speed. (**d**) Slip.

In terms of slip ratio control, as shown in Figure 8d, there is no overshooting phenomenon in ADRC, and the response time of ADRC to reach the steady-state value is faster than that of SMC and PID. The comparison of the braking effects of the different ABS control strategies involves multiple factors. On snowy roads, the advantages of the ADRC strategy in terms of braking distance and braking time are not significant. However, considering the overall controller's response time, the results show that the ADRC algorithm offers superior control performance.

5.2.3. Variable Pavement Braking

To verify the adaptability of the control strategies, a complex variable surface condition was selected, transitioning from dry asphalt to a snowy road. Braking began on dry asphalt, and after 1 s of braking, the road surface switched to snow. Figure 9 shows the braking performance of the three ABS control strategies, ADRC, SMC, and PID, under variable road conditions. From Figure 9a, it can be observed that the ADRC strategy provides a shorter braking distance, thereby enhancing safety. Figure 9b,c indicates that on dry asphalt, both ADRC and SMC achieve similar effects in terms of reducing speed. However, when the road surface changes, PID control exhibits overshooting, while ADRC adjusts more quickly than SMC.
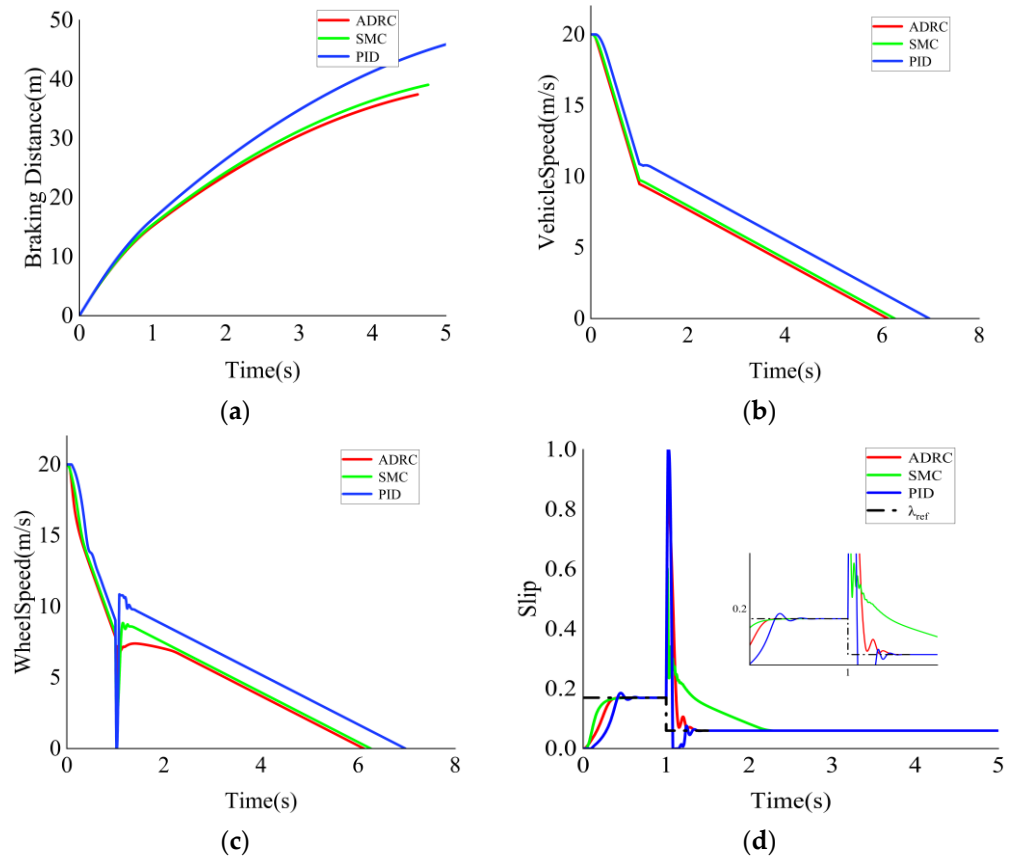
Figure 9. Braking performance on variable pavement. (**a**) Braking distance. (**b**) Vehicle speed. (**c**) Wheel speed. (**d**) Slip.

Figure 9d demonstrates that in terms of slip ratio control, during sudden changes in road conditions, the response times of SMC and PID both lag behind those of ADRC. Moreover, ADRC reaches a steady state and outputs the optimal slip ratio faster than the other two methods. This indicates that PID and SMC have poorer adaptability to variable road conditions, whereas ADRC shows stronger adaptability and better robustness to changes in road surfaces. Considering factors such as braking time, braking distance, and control response time, the ADRC strategy performs better compared to PID and SMC. It significantly improves vehicle stability and safety during braking.

6. Conclusions

The braking performance of a vehicle during emergency braking is influenced by both road surface conditions and the robustness of the controller. A hierarchical control strategy for an anti-lock braking system (ABS) employing active disturbance rejection control (ADRC) has been proposed. The main conclusions are as follows:

- The force acting on a single wheel and the road–tire model were analyzed. For the EMB system, a road recognition algorithm based on an extended state observer (ESO) was designed. During emergency braking conditions, this algorithm observes the current longitudinal vehicle speed to obtain the current slip ratio. By calculating the utilization adhesion coefficient for typical road surfaces and comparing it with the actual road surface adhesion coefficient, the algorithm identifies the road type. This approach meets the requirements for road recognition accuracy and response time during emergency braking scenarios;

- Through ABS braking simulations, the designed ADRC-based slip ratio tracking control strategy for ABS was validated. Compared to the PID and SMC algorithms, the

ADRC strategy demonstrates superior performance across various road conditions, when considering factors such as overall braking distance, braking time, and control response. Under single-pavement conditions, compared to PID control, the braking distance is reduced by approximately 5.1%, and the braking time is shortened by 4.3%; compared to SMC, the braking distance is reduced by 4.2%, and the braking time is shortened by 1.6%. Under variable pavement conditions, compared to PID control, the braking distance is reduced by 22.5%, and the braking time is shortened by 10.3%; compared to SMC, the braking distance is reduced by 6%, and the braking time is shortened by 3.2%. ADRC exhibits strong robustness and better adaptability to changes in road surfaces, which is crucial for enhancing vehicle braking performance.

Author Contributions: Conceptualization, S.L.; Methodology, S.L.; Software, B.Z.; Validation, B.Z.; Formal analysis, B.Z.; Investigation, J.M.; Resources, X.Z.; Writing—original draft, B.Z.; Writing—review & editing, B.Z.; Project administration, X.Z. All authors have read and agreed to the published version of the manuscript.

Data Availability Statement: The original contributions presented in this study are included in the article. Further inquiries can be directed to the corresponding author.

Conflicts of Interest: The authors declare no conflict of interest.

Abbreviations

The following abbreviations are used in this manuscript:

ABS	Anti-lock braking system
EMB	Electro-mechanical braking system
ESO	Extended state observer
ADRC	Active disturbance rejection control
SMC	Sliding-mode control

References

1. Mortazavizadeh, S.A.; Ghaderi, A.; Ebrahimi, M.; Hajian, M. Recent Developments in the Vehicle Steer-by-Wire System. *IEEE Trans. Transp. Electrif.* **2020**, *6*, 1226–1235. [CrossRef]
2. Li, C.; Zhuo, G.; Tang, C.; Xiong, L.; Tian, W.; Qiao, L.; Cheng, Y.; Duan, Y. A Review of Electro-Mechanical Brake (EMB) System: Structure, Control and Application. *Sustainability* **2023**, *15*, 4514. [CrossRef]
3. Hua, X.; Zeng, J.; Li, H.; Huang, J.; Luo, M.; Feng, X.; Xiong, H.; Wu, W. A Review of Automobile Brake-by-Wire Control Technology. *Processes* **2023**, *11*, 994. [CrossRef]
4. Li, W.; Wang, M.; Huang, C.; Li, B. A Survey of Hybrid Braking System Control Methods. *World Electr. Veh. J.* **2024**, *15*, 372. [CrossRef]
5. Ji, Q.; Zheng, L.; Bi, Y.; Pang, H. Review of Brake-by-Wire Technology for Low-Speed and Autonomous Vehicles. *World Electr. Veh. J.* **2024**, *15*, 581. [CrossRef]
6. Gong, X.; Ge, W.; Yan, J.; Zhang, Y.; Gongye, X. Review on the Development, Control Method and Application Prospect of Brake-by-Wire Actuator. *Actuators* **2020**, *9*, 15. [CrossRef]
7. Yu, D.; Wang, W.; Zhang, H.; Xu, D. Research on Anti-Lock Braking Control Strategy of Distributed-Driven Electric Vehicle. *IEEE Access* **2020**, *8*, 162467–162478. [CrossRef]
8. Elghitany, M.N.; Tolba, F.; Mohamed Abdelkader, A. Low Vehicle Speeds Regenerative Anti-lock Braking System. *Ain Shams Eng. J.* **2022**, *13*, 101570. [CrossRef]
9. Kirpalsinh, R.; Jeet, P.; Dhruv, T.; Nisarg, P.; Dhaval, P.; Sahil, R.; Mihir, R.; Bhavik, P. A Review on Automobile Safety Technology in ABS. *Int. J. Innov. Res. Technol.* **2019**, *6*, 120–124.
10. Xue, X.; Cheng, K.W.E. Electric Antilock Braking Systems for Electric Vehicles. In Proceedings of the 2020 8th International Conference on Power Electronics Systems and Applications (PESA), Hong Kong, China, 7–10 December 2020; pp. 1–6.
11. Wang, Y.; Lv, C.; Yan, Y.; Peng, P.; Wang, F.; Xu, L.; Yin, G. An Integrated Scheme for Coefficient Estimation of Tire–Road Friction With Mass Parameter Mismatch Under Complex Driving Scenarios. *IEEE Trans. Ind. Electron.* **2022**, *69*, 13337–13347. [CrossRef]

12. Li, B.; Wenjuan, E.; Feng, T.; Ding, Y.; Li, Y.; Wang, X.; Jiang, X.; Shen, C. Road Adhesion Coefficient Estimation Based on LiDAR Reflectance Intensity. *IEEE Sens. J.* **2024**, *24*, 29135–29148. [CrossRef]

13. Sun, X.; Xiao, Z.; Wang, Z.; Zhang, X.; Fan, J. Acceleration Slip Regulation Control Method for Distributed Electric Drive Vehicles under Icy and Snowy Road Conditions. *Appl. Sci.* **2024**, *14*, 6803. [CrossRef]

14. Zhu, S.; Fan, X.; Qi, G.; Wang, P. Review of control algorithms of vehicle anti-lock braking system. *Recent Pat. Eng.* **2023**, *17*, 30–45. [CrossRef]

15. Xu, Z.; Lu, Y.; Chen, N.; Han, Y. Integrated Adhesion Coefficient Estimation of 3D Road Surfaces Based on Dimensionless Data-Driven Tire Model. *Machines* **2023**, *11*, 189. [CrossRef]

16. Salma, K.; Mehdi, M.E.; Houcine, C. Intelligent Global Sliding Mode Control of Anti-Lock Braking System Using Optimization Algorithms. In Proceedings of the 2024 4th International Conference on Innovative Research in Applied Science, Engineering and Technology (IRASET), FEZ, Morocco, 16–17 May 2024; pp. 1–7.

17. Meléndez-Useros, M.; Jiménez-Salas, M.; Viadero-Monasterio, F.; Boada, B.L. Tire Slip H∞ Control for Optimal Braking Depending on Road Condition. *Sensors* **2023**, *23*, 1417. [CrossRef]

18. Fareh, R.; Khadraoui, S.; Abdallah, M.Y.; Baziyad, M.; Bettayeb, M. Active disturbance rejection control for robotic systems: A review. *Mechatronics* **2021**, *80*, 102671. [CrossRef]

19. Guo, B.; Bacha, S.; Alamir, M. A review on ADRC based PMSM control designs. In Proceedings of the IECON 2017—43rd Annual Conference of the IEEE Industrial Electronics Society, Beijing, China, 29 October–1 November 2017; pp. 1747–1753.

20. Cao, Y.; Cao, Z.; Feng, F.; Xie, L. ADRC-Based Trajectory Tracking Control for a Planar Continuum Robot. *J. Intell. Robot. Syst.* **2023**, *108*, 1. [CrossRef]

21. Li, W.; Zhang, Q.; Zhang, Y. The Effect of ADRC on Vehicle Braking Performance. *J. Electr. Eng. Technol.* **2020**, *15*, 705–712. [CrossRef]

22. Aksjonov, A.; Augsburg, K.; Vodovozov, V. Design and Simulation of the Robust ABS and ESP Fuzzy Logic Controller on the Complex Braking Maneuvers. *Appl. Sci.* **2016**, *6*, 382. [CrossRef]

23. He, R.; Zhang, L. Interval recognition algorithm of the pavement surface condition based on Lagrange interpolation method. *Math. Probl. Eng.* **2020**, *2020*, 4251027. [CrossRef]

24. Wang, B.; Guan, H.; Lu, P.; Zhang, A. Road surface condition identification approach based on road characteristic value. *J. Terramechanics* **2014**, *56*, 103–117. [CrossRef]

25. Bin, M.; Marconi, L. Model Identification and Adaptive State Observation for a Class of Nonlinear Systems. *IEEE Trans. Autom. Control* **2021**, *66*, 5621–5636. [CrossRef]

26. Avzayesh, M.; Al-Masri, W.; Abdel-Hafez, M.F.; AlShabi, M. Improved-Performance Vehicle's State Estimator Under Uncertain Model Dynamics. *IEEE Open J. Instrum. Meas.* **2024**, *3*, 8500112. [CrossRef]

27. Salas, M.J.; Useros, M.M.; Monasterio, F.V.; López, M.J.; Boada, B.L.B. Simultaneous Robust H∞ Output-Feedback Control and Sensor Fault Estimation for Path Tracking. In Proceedings of the FISITA 2023 World Congress, Barcelona, Spain, 12–15 September 2023.

28. Huang, Y.; Han, J. Analysis and design for the second order nonlinear continuous extended states observer. *Chin. Sci. Bull.* **2000**, *45*, 1938–1944. [CrossRef]

29. Peng, X.; Jia, M.; He, L.; Yu, X.; Lv, Y. Fuzzy sliding mode control based on longitudinal force estimation for electro-mechanical braking systems using BLDC motor. *CES Trans. Electr. Mach. Syst.* **2018**, *2*, 142–151. [CrossRef]

30. Hote, Y.V.; Jain, S. Generalized Active Disturbance Rejection Control: Review, Applications and Challenges. In Proceedings of the 2021 IEEE International Conference on Automation/XXIV Congress of the Chilean Association of Automatic Control (ICA-ACCA), Valparaíso, Chile, 22–26 March 2021; pp. 1–6.

31. Han, J. From PID to Active Disturbance Rejection Control. *IEEE Trans. Ind. Electron.* **2009**, *56*, 900–906. [CrossRef]

32. Wang, Z.; Li, J.; Duan, D. Manipulation strategy of tilt quad rotor based on active disturbance rejection control. *Proc. Inst. Mech. Eng. Part G J. Aerosp. Eng.* **2020**, *234*, 573–584. [CrossRef]